Journal of
Synchrotron
Radiation

ISSN 0909-0495

Received 31 July 2007
Accepted 19 August 2008

An access to buried interfaces: the X-ray reflectivity set-up of BL9 at DELTA

Michael Paulus,[a]* Daniela Lietz,[a] Christian Sternemann,[a] Kaveh Shokuie,[a] Florian Evers,[a] Metin Tolan,[a] Claus Czeslik[b] and Roland Winter[b]

[a]Fakultät Physik/DELTA, Technische Universität Dortmund, D-44221 Dortmund, Germany, and [b]Fakultät Chemie, Physikalische Chemie I, Techische Universität Dortmund, D-44227 Dortmund, Germany. E-mail: michael.paulus@tu-dortmund.de

An X-ray reflectivity set-up to study buried interfaces at beamline BL9 of the electron storage ring DELTA is presented. The structure of solid–gas and solid–liquid interfaces can be investigated using X-rays with incident energies of about 27 keV. A detailed description of the set-up is given and its performance is demonstrated by a discussion of selected applications, *i.e.* protein adsorption at the solid–liquid interface and gas adsorption at the solid–gas interface at elevated pressures.

Keywords: X-ray reflectivity; solid–liquid interfaces; beamline.

1. Introduction

The X-ray reflectivity technique is a powerful method for surface characterization and is utilized for scientific and industrial applications. Thus, a lot of compact X-ray diffractometers equipped with copper or molybdenum X-ray tubes are accessible on the market and widely used for standard sample characterization. However, the vast majority of scientific applications requiring, for example, high photon flux, defined polarization, high resolution or a dedicated photon energy make the use of synchrotron radiation mandatory. Examples are anomalous scattering where element-sensitive reflectivities can be performed (see, for example, Sloutskin *et al.*, 2007; Fänle *et al.*, 2007; Park *et al.*, 2005; DiMasi *et al.*, 2001) or scattering at buried interfaces where high-energy photons with high penetration depth are utilized to investigate solid–liquid and solid–solid interfaces (see, for example, Lefenfeld *et al.*, 2006; Mezger *et al.*, 2006; Engemann *et al.*, 2004; Rieutord *et al.*, 2001; Reichert *et al.*, 2000). In particular, the study of liquid–liquid interfaces has become an important research area in the past years (Lin *et al.*, 2003; Tikhonov *et al.*, 2006; Luo *et al.*, 2006) which requires both a huge photon flux at high energy and a highly specialized sample environment. A large penetration length is also achieved using neutrons. The combination with the possibility of deuteration of biological samples for scattering contrast variation makes neutron reflectivity measurements in particular an important tool for biological applications. For an overview see, for instance, Fragneto-Cusani (2001) or Daillant & Gibaud (1999). A large body of experimental work has been performed investigating solid–liquid or membrane–liquid interfaces simulating cell environments. However, neutron reflectivities are limited by the low incoming neutron flux in comparison with synchrotron radiation. X-ray reflectivity measurements can overcompensate the limited wave vector range of neutron reflectivity experiments, although the electron density contrast in biological systems such as aqueous protein solutions is low.

In this work an X-ray reflectivity set-up to study buried interfaces with 27 keV photons is presented. This set-up at beamline BL9 of the synchrotron radiation source DELTA allows the characterization of buried interfaces which are not accessible by X-ray tubes because of the demand of high photon flux at energies above 20 keV. Although this kind of instrumentation is not particular new, it shows a valuable extension to the existing but rare high-energy reflectivity set-ups at the high-flux third-generation synchrotron light sources like the ESRF, APS and SPring-8.

The paper is organized as follows. In the second section the X-ray reflectivity technique is briefly introduced followed by an experimental section describing the beamline, the reflectivity set-up and sample environments. Finally, selected experiments will be presented and discussed in order to demonstrate the performance of the technique.

2. X-ray reflectivity

An overview of the X-ray reflectivity technique can be found by Daillant & Gibaud (1999) and Tolan (1999). Because of the symmetric arrangement of the incoming and reflected beam in an X-ray reflectivity experiment, the wavevector transfer is vertical with respect to the sample surface and is given by $q_z = (4\pi/\lambda)\sin(\alpha)$. Here, λ is the wavelength of the X-rays and α is the incidence scattering angle of the incoming beam. Thus a reflectivity measurement provides information about the laterally averaged vertical electron density profile. The scattered intensity in an X-ray reflectivity experiment can be

calculated *via* the first Born approximation. The reflectivity R is defined by (Braslau *et al.*, 1988)

$$R = R_{\rm F}\left|\int (\mathrm{d}\rho/\mathrm{d}z)\exp(iqz)\,\mathrm{d}z\right|^2, \qquad (1)$$

with the Fresnel reflectivity $R_{\rm F}$ and electron density profile $\rho(z)$ (Als-Nielsen & McMorrow, 2004). Thus the reflectivity is predominantly sensitive to the change in electron density. In contrast to layer formation at the gas–solid or gas–liquid interfaces the corresponding high density contrast is usually strongly reduced for layers at a liquid–solid interface. This loss of density contrast makes the investigation of biological systems under natural conditions difficult. For example, the difference in the dispersion δ, which is proportional to the electron density ρ according to $\delta = r_{\rm e}\rho\lambda^2/(2\pi)$ with $r_{\rm e}$ denoting the classical electron radius, between lysozyme molecules and the aqueous solvent is only $\Delta\delta = 0.2$ while the contrast to the gas atmosphere is $\Delta\delta = 1.2$.

3. Set-up for the investigation of buried interfaces

In the following sections the beamline BL9 at the synchrotron source DELTA will be described as well as the reflectivity set-up and the sample environment. DELTA is an electron storage ring which operates with an electron energy of 1.5 GeV. The maximum electron current is 130 mA with an average lifetime of about 10 h. For further information see, for example, Tolan *et al.* (2003) and Berges *et al.* (2007).

3.1. Beamline BL9, experimental endstations and reflectivity set-up

The photon source of beamline BL9 is a superconducting asymmetric wiggler, one of the three insertion devices of DELTA. The critical energy of the wiggler is 7.9 keV. The beamline is equipped with a silicon (311) double-crystal monochromator with an energy resolution of $\Delta E/E = 10^{-4}$. The horizontal focusing of the photon beam is attended by sagittal bending of the second monochromator crystal leading to a beam width of 1 mm on the sample position, while vertical focusing is not applied. Owing to the monochromator design the maximum photon energy accessible by the (311) optics is 30 keV. For detailed information about beamline BL9, see Krywka *et al.* (2006).

At this beamline, three different endstations are available: a Rowland-type spectrometer which allows spectroscopy experiments such as fluorescence analysis, non-resonant inelastic X-ray scattering and absorption spectroscopy (Enkisch *et al.*, 2004; Sternemann *et al.*, 2003); a small-angle scattering set-up (Krywka *et al.*, 2007; Javid *et al.*, 2007); and a six-circle diffractometer which is designed for surface diffraction as well as powder diffraction and texture analysis (Krywka *et al.*, 2006).

For high-energy X-ray reflectivity measurements at an energy of 27 keV a typical photon flux of 7×10^8 photons s^{-1} mm^{-2} at 100 mA is obtained. The energy of 27 keV is a compromise between energy and flux; additionally the damage of biological material like proteins by the radiation is minimized in the energy region around 25 keV (Reich *et al.*, 2005). A sketch of the reflectivity set-up is shown in Fig. 1.

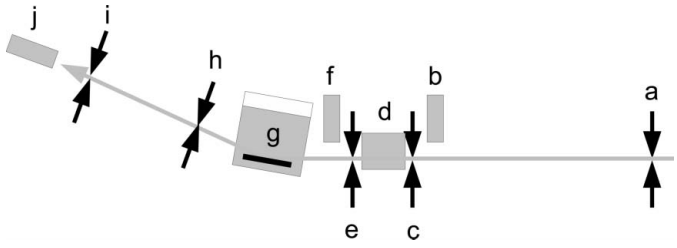

Figure 1
Experimental set-up for the high-energy X-ray reflectivity measurements. *a*, slit system; *b*, NaI normalization detector; *c*, slit system; *d*, auto-absorber system and fast shutter (XIA); *e*, slit system; *f*, NaI normalization detector; *g*, sample cell; *h*, slit system; *i*, slit system; *j*, NaI detector.

The incoming photon beam is collimated by two slit systems (*a*, *c*) and is finally defined by a third slit system (*e*) to a vertical height of 0.2 mm. Thus the beam size at the sample position is 1 mm × 0.2 mm. An auto-absorber/fast shutter system (*d*) with Ag foils mounted in front of the third slit system is used for flux limitation. This feature is fully implemented in the beamline software and is used automatically during a reflectivity measurement. Two NaI detectors monitor the incoming flux before (*b*) and behind (*f*) the auto-absorber system. The sample cells (*g*) are placed in the six-circle diffractometer 200 mm behind the beam-defining slit system and 300 mm before the first detector slit system (*h*) which suppresses the diffuse scattered radiation. The final slit system (*i*), which defines the angular resolution, is placed close before the NaI detector (*j*) measuring the reflected intensity at a distance of 1000 mm from the sample. Typically the angular resolution is about 0.015° and a high-energy reflectivity measurement over seven orders of magnitude takes 60 min including a longitudinal diffuse scan. Typical raw X-ray reflectivity data together with a longitudinal diffuse scan of a Si-aqueous lysozyme solution interface are shown in Fig. 3. The background level is increased by one order of magnitude which is due to scattering at the liquid phase which is penetrated by the X-rays.

3.2. Sample environments

3.2.1. Solid–liquid interfaces. For the study of solid–liquid interfaces a small sample cell with a volume of about 5 cm^3 was built. Investigating the solid–liquid interface, neither a miniscus at the interface forms nor the contact angle of the liquid at the cell wall affects the experiment in contrast to set-ups dealing with liquid–liquid interfaces (Mitrinovic *et al.*, 1999). Thus, the sample cell can be built as small as possible and no tilt of the cell walls is required. A picture of the sample cell is displayed in the inset of Fig. 2. The sample cell has two Kapton windows for beam entrance and exit. A wafer, *e.g.* silicon, can be placed in a sample carrier which assures a stable position of the wafer during the measurement. The sample cell can be fixed on a heat exchanger for temperature control. It is filled by the liquid in order to create a solid–liquid interface.

Table 1
X-ray attenuation lengths for different materials at a photon energy E_{ph} = 27 keV.

Values calculated using http://henke.lbl.gov/optical_constants/.

Material	Formula	Attenuation length (mm)
Octane	C_8H_{18}	55.8
Polypropylene	C_3H_6	43.6
Water	H_2O	26.4
Glycerol	$C_3H_8O_3$	24.5
Graphite	C	19.1
Diamond	C	12.0
Teflon	C_2F_4	11.0
Aluminium	Al	2.8
Silicon	Si	2.5
Iron	Fe	0.1

During an X-ray reflectivity measurement the sample cell is tilted to change the angle of incidence. The incoming radiation enters the liquid at the Kapton windows close to 90°. The total length of the beam path through the liquid sample is about 30 mm. This results in a transmission of 32% in the case of water at a photon energy of 27 keV. Attenuation lengths are summarized in Table 1 for different samples giving an estimate of possible systems which can be measured with this set-up.

3.2.2. Pressure cell. The pressure cell is constructed for investigations of sample surfaces under gas pressures up to 40 bar. A photograph of the pressure cell is shown in Fig. 2. It consists of a stainless steel cell with an inner diameter of 124 mm, and the wall thickness is about 20 mm. The cell volume is 500 cm^3. For applications requiring gas pressures between 3 bar and 40 bar, two aluminium windows with a width of 5 mm, height of 28 mm and 1 mm thickness are bolted on each side of the cell. The transmission of each window at 27 keV is 70%. For lower pressures (less than 6 bar) the aluminium windows can be replaced by Kapton windows. For thermal stability, the sample cell is mounted on a heat exchanger. A Lakeshore control unit regulates the sample temperature by driving a heating foil, leading to a temperature stability of ± 0.02 K. The cell cover is equipped with lead-throughs for temperature sensors (Pt100), and gas input and output. For the investigation of gas–liquid interfaces the whole bottom of the sample cell, which is encircled by a 0.5 mm-high edge, can be covered by the liquid. For the study of solid–gas interfaces or solid–liquid interfaces under pressure, the small sample holder described in the last paragraph can be placed in the middle of the pressure cell, stabilized by an adapter plate.

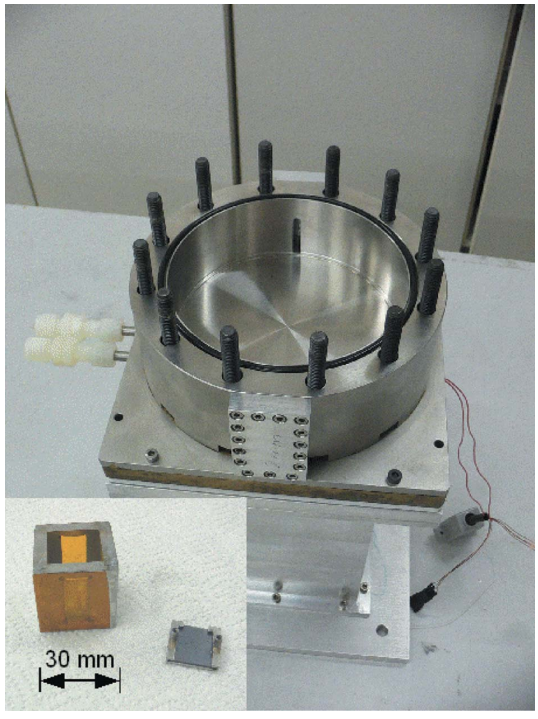

Figure 2
The pressure cell mounted on the heat exchanger. On the left side the connectors for the cooling liquid are visible. In front and at the back wall the two aluminium windows are connected. Inside the cell the small edge which holds the liquid is shown. The inset shows a photograph of the small sample cell for the investigation of solid–liquid interfaces. The sample carrier which holds the wafer is placed besides the sample cell.

4. Applications

In the following section, two selected experiments will be presented to give a short overview regarding possible applications. First, protein adsorption at solid–liquid interface is discussed for aqueous lysozyme solutions. This is followed by an investigation of the carbon dioxide adsorption at the solid–gas interface at elevated pressures. These experiments were conducted employing the reflectivity set-up described in §3.

4.1. Protein adsorption at the solid–liquid interface

A large body of work has been performed dealing with the properties of bulk protein solutions as a function of different environmental parameters such as temperature, pressure and protein concentration (Winter & Köhling, 2004; Merzel & Smith, 2002; Woenckhaus *et al.*, 2001; Panick *et al.*, 1998; Sosnick & Trewhella, 1992). However, in natural cell environments proteins are often confined by membranes which serve as an interface between the intracellular and extracellular regions. Additional lipid membranes and macromolecular interfaces are present intracellularly in eukaryotes. Theoretical work shows that the confinement has a drastic effect on the protein. Beside the formation of thin protein layers at such interfaces which are controlled by entropic and enthalpic interactions and density fluctuations at the interface, a change in conformation can be triggered by the presence of the interface which can even lead to aggregation (Czeslik, 2004; Zhou & Dill, 2001; Minton, 2000; Lu *et al.*, 1998; Su *et al.*, 1998). Thus, the investigation of protein solutions near interfaces will also yield important information about biological processes. In this work an investigation of the aqueous-lysozyme-solution–silicon interface is presented. Adsorption of lysozyme layers at solid–liquid interfaces was found for low-concentrated lysozyme solutions by neutron reflectivity studies (Su *et al.*, 1998; Ravindra *et al.*, 2004). These neutron

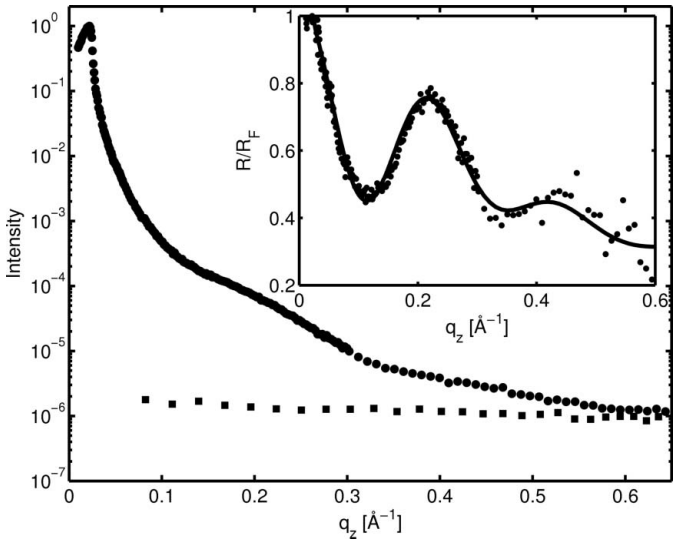

Figure 3
Raw X-ray reflectivity data (circles) and diffuse scan (squares) of the aqueous-lysozyme-solution–silicon interface measured at pH 7. The inset shows the logarithm of the reflectivity normalized by the Fresnel reflectivity. The solid curve shows a refinement of the data assuming a 28 Å-thick lysozyme layer on the silicon surface which is equivalent to the formation of a protein monolayer.

reflectivity studies propose monolayer or bilayer adsorption. However, the q range was rather limited in this experiment.

The X-ray reflectivity measurements were performed using the small sample cell and the set-up described above. Lysozyme from Sigma-Aldrich was utilized in NaH_2PO_4 buffer solution at pH 7. The concentration was 10 mmol l^{-1}. The raw X-ray reflectivity data and longitudinal diffuse scan are presented in Fig. 3. The inset of Fig. 3 shows the reflectivity normalized by the Fresnel reflectivity. The oscillation indicates the formation of a layer at the solid–liquid interface. The reflectivity was refined using the Parratt algorithm (Parratt, 1954) leading to a layer thickness of 28 $\pm$ 2 Å and a roughness of 5.1 $\pm$ 1.5 Å. The corresponding dispersion profile is displayed in Fig. 4. Here the low density contrast between the layer and liquid phase becomes clearly visible. The layer thickness, roughness and the density contrast to the liquid phase indicate formation of a monolayer of procumbent lysozyme molecules, taking into account the reported literature value of the molecule's diameter of about 30 Å and the electron density contrast between a lysozyme molecule and the liquid, which is about 30% (Svergun *et al.*, 1998). It should be noted that the q range of the experiment is three times larger than for neutron experiments at similar interfaces leading to a much higher accuracy resolving the protein layer thickness. However, the observed q range is still too small to resolve small changes in the shape of the electron density profile. Such changes can be studied using the corresponding instruments at the third-generation synchrotron light sources ESRF, APS or SPring-8.

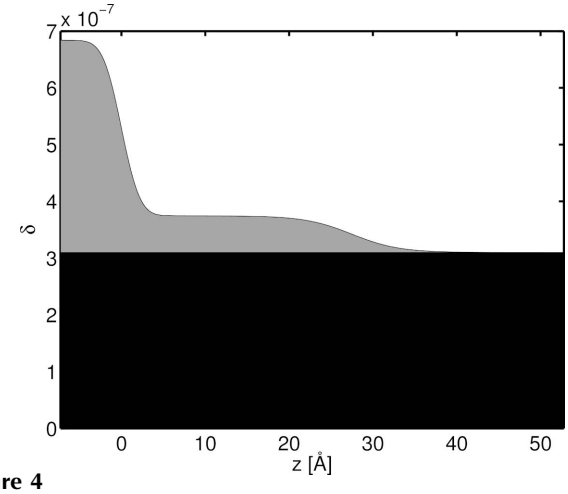

Figure 4
Dispersion profile of the aqueous-lysozyme-solution–silicon interface obtained by a refinement of the reflectivity data. For a better visualization of the low dispersion contrast of the lysozyme layer to the liquid phase, the dispersion on the liquid phase is not subtracted but marked as a black area.

4.2. Adsorption of CO_2 at the solid–gas interface

In the natural environment surfaces are partially covered by gas molecules of the surrounding atmosphere. This adsorption layer can influence the surface properties significantly. Thus a detailed understanding of the structure of liquid–gas or solid–gas interfaces is of fundamental importance for material science. By the use of a Lifshitz-theory-based approach the adsorbed layer thickness as a function of the gas pressure, the so-called adsorption isotherm, is given by Adamson (1997),

$$l_{\rm m} = \left[\frac{A_{\rm eff}}{6\pi\Delta\rho_T k_{\rm B} T \log(p/p_0)}\right]^{1/3}, \qquad (2)$$

where $k_{\rm B}$ is the Boltzmann factor, p is the gas pressure, p_0 is the condensation pressure of the gas at a given temperature T, and $\Delta\rho_T$ is the particle difference between the liquid (film) and the gas phase. $A_{\rm eff}$ is the effective Hamaker constant which is a measure of the interaction strength between the substrate and the adsorbed film. The pressure dependence of the film thickness $l_{\rm m}$ accords to a Frenkel–Halsey–Hill (FHH) isotherm (Frenkel, 1946; Halsey, 1948; Hill, 1949). An approximation of $A_{\rm eff}$ can be calculated using Lifshitz theory (Israelachvili, 2000).

Using a conventional X-ray diffractometer with copper $K\alpha$ radiation the window material of a pressure cell is limited on transparent materials like Kapton or Mylar. This limits the measurements up to a pressure of approximately 5 bar (Paulus *et al.*, 2005). Thus, only sample systems with a low absorption and low condensation pressure can be measured. The use of aluminium windows for pressure cells in combination with high photon energies allows higher pressures, so that a huge variety of systems with respect to their phase diagram can be investigated.

In this work the adsorption of CO_2 on a silicon substrate is discussed. For the measurements the pressure cell described above was used. A wafer was placed in the small sample cell which was positioned in the middle of the pressure cell. First, the pressure cell was filled with helium and a reference reflectivity of the solid–gas interface was recorded. After

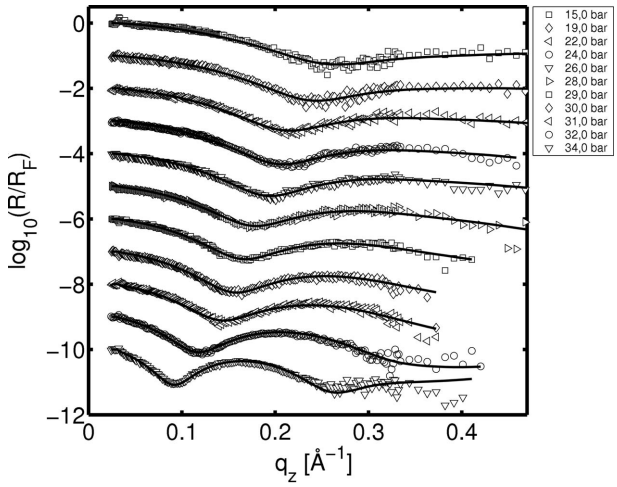

Figure 5
Logarithm of the X-ray reflectivities normalized by the Fresnel reflectivity from the CO_2–silicon interface. For better visualization the reflectivies are shifted vertically. Refinements of the reflectivities are shown as solid lines.

recording the reflectivity the cell was purged for several minutes with CO_2 (purity 99.995%) to displace the helium atmosphere. The temperature in the sample cell was set to 273 K leading to a condensation pressure of $p_0 = 35$ bar. After temperature stabilization ($\Delta T \simeq 0.02$ K), reflectivities of the silicon–CO_2 interface were recorded at different pressures. In Fig. 5 reflectivities normalized by the Fresnel reflectivity of the silicon–CO_2 interface are shown. For better visualization the reflectivities are shifted vertically. The Kiessig fringes are visible especially at high pressures. The reduction of the oscillation period with rising pressure indicates a growth of layer thickness with rising pressure. The reversibility of the adsorption process was proved by recording reflectivity scans after pressure drop and subsequent realignment of pressure to the old value. No changes in the reflectivity curves were observed. The reflectivities were refined using the effective density model (Tolan, 1999). The refinements of the reflectivities are also shown in Fig. 5 as solid lines. The resulting layer thicknesses as a function of the gas pressure are presented in Fig. 6. A typical shape of a FHH isotherm is obtained.

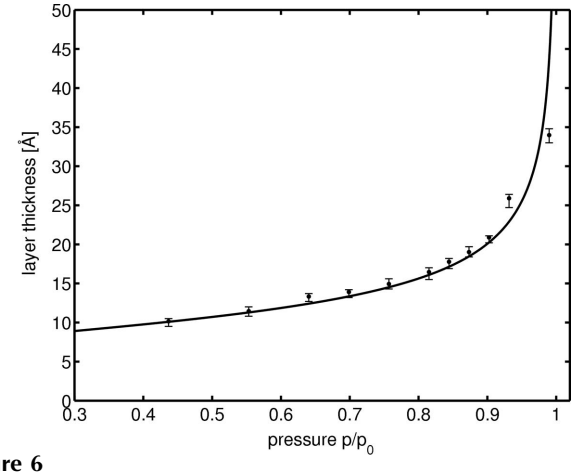

Figure 6
Adsorption isotherm of the system CO_2 on silicon. The film thickness is displayed as a function of normalized pressure p/p_0 where p_0 is the condensation pressure at $T = 273$ K. The solid line is a refinement of equation (2) leading to an effective Hamaker constant of $A_{\rm eff} = (-7.9 \pm 1) \times 10^{-19}$ J.

This adsorption isotherm was refined using equation (2). The result is shown in Fig. 6 as a solid line and leads to an effective Hamaker constant of $A_{\rm eff} = (-7.9 \pm 1) \times 10^{-19}$ J. A calculation of the effective Hamaker constant using a Lifshitz-based approach leads to a value of $A_{\rm eff}^{\rm th} = -2.3 \times 10^{-19}$ J. This deviation between the experimental and theoretical value is consistent with other measurements where a shift of the experimental Hamaker constant to lower values was found (Paulus *et al.*, 2005, 2008; Shokuie *et al.*, 2007).

5. Summary

In summary, an X-ray reflectivity set-up to study buried interfaces at beamline BL9 at the synchrotron light source DELTA has been presented. X-ray reflectivities can be measured at a photon energy of 27 keV which implies high penetration depth in solid or liquid samples. A short overview of the sample environments for the investigation of solid–liquid interfaces and solid–gas interfaces under pressure has been presented. The successful operation of the set-up was demonstrated by the discussion of two examples, the investigation of the silicon–aqueous-lysozyme-solution and the silicon–CO_2 interface under different gas pressures. The investigation of the silicon–aqueous-lysozyme-solution interface indicates the formation of a monolayer of lysozyme at the interface. The pressure-dependent investigation of the CO_2 silicon interface yields to the determination of the effective Hamaker constant, which is a measure of the coupling between the thin adsorbed film and the silicon substrate.

The authors acknowledge the DELTA machine group for providing the synchrotron radiation and technical support.

References

Adamson, A. W. (1997). *Physical Chemistry of Surfaces.* New York: John Wiley and Sons.
Als-Nielsen, J. & McMorrow, D. (2004). *Elements of Modern X-ray Physics.* New York: John Wiley and Sons.
Berges, U., Sternemann, C., Tolan, M., Westphal, C., Weis, T. & Wille, K. (2007). *AIP Conf. Proc.* **879**, 30–33.
Braslau, A., Pershan, P. S., Swislow, G., Ocko, B. M. & Als-Nielsen, J. (1988). *Phys. Rev. A*, **38**, 2457–2470.
Czeslik, C. (2004). *Z. Phys. Chem.* **218**, 771–801.
Daillant, J. & Gibaud, A. (1999). *X-ray and Neutron Reflectivity: Principles and Applications.* Paris: Springer.
DiMasi, E., Tostmann, H., Shpyrko, O. G., Huber, P., Ocko, B. M., Pershan, P. S., Deutsch, M. & Berman, L. E. (2001). *Phys. Rev. Lett.* **86**, 1538.
Engemann, S., Reichert, H., Dosch, H., Bilgram, J., Honkimäki, V. & Snigirev, A. (2004). *Phys. Rev. Lett.* **92**, 205701.
Enkisch, H., Sternemann, C., Paulus, M., Volmer, M. & Schülke, W. (2004). *Phys. Rev. A*, **70**, 022508.
Fänle, M., Steinauf, D., Martosiswoyo, L., Goering, E., Brück, S. & Schütz, D. (2007). *Phys. Rev. B*, **75**, 144415.
Fragneto-Cusani, G. (2001). *J. Phys. Condens. Matter*, **13**, 4973–4989.

Frenkel, J. (1946). *Kinetic Theory of Liquids.* Oxford University Press.
Halsey, G. D. (1948). *J. Chem. Phys.* **16**, 931.
Hill, T. L. (1949). *J. Chem. Phys.* **17**, 590.
Israelachvili, J. (2000). *Intermolecular and Surface Forces*, 2nd ed. San Diego: Academic Press.
Javid, N., Vogt, K., Krywka, C., Tolan, M. & Winter, R. (2007). *Chem. Phys. Chem.* **8**, 679–689.
Krywka, C., Paulus, M., Sternemann, C., Volmer, M., Remhof, A., Nowak, G., Nefedov, A., Pöter, B., Spiegel, M. & Tolan, M. (2006). *J. Synchrotron Rad.* **13**, 8–13.
Krywka, C., Sternemann, C., Paulus, M., Javid, N., Winter, R., Al-Sawalmih, A., Yi, S., Raabe, D. & Tolan, M. (2007). *J. Synchrotron Rad.* **14**, 244–251.
Lefenfeld, M., Baumert, J., Sloutskin, E., Kuzmenko, I., Pershan, P., Deutsch, M., Nuckolls, C. & Ocko, B. M. (2006). *Proc. Natl. Acad. Sci.* **103**, 2541–2545.
Lin, B., Meron, M., Gebhardt, J., Graber, T., Schlossman, M. L. & Viccaro, P. J. (2003). *Physica B*, **336**, 75–80.
Lu, J. R., Su, T. J., Thirtle, P. N., Thomas, R. K., Rennie, A. R. & Cubitt, R. (1998). *J. Colloid Interf. Sci.* **206**, 212–223.
Luo, G., Malkova, S., Yoon, J., Schultz, D. G., Lin, B., Meron, M., Benjamin, I., Vanysek, P. & Schlossman, M. L. (2006). *Science*, **311**, 216–218.
Merzel, F. & Smith, J. C. (2002). *Proc. Natl. Acad. Sci. USA*, **99**, 5378–5383.
Mezger, M., Reichert, H., Schöder, S., Okasinski, J., Schröder, H., Dosch, H., Palms, D., Ralston, J. & Honkimäki, V. (2006). *Proc. Nat. Acad. Sci. USA*, **103**, 18401–18404.
Minton, A. P. (2000). *Biophys. J.* **78**, 101–109.
Mitrinovic, D. M., Zhang, Z., Williams, S. M., Huang, Z. & Schlossman, M. L. (1999). *J. Phys. Chem. B*, **103**, 1779–1782.
Panick, G., Malessa, R., Winter, R., Rapp, G., Frye, K. J. & Royer, C. (1998). *J. Mol. Biol.* **275**, 389–402.
Park, C., Fenter, P. A., Sturchio, N. C. & Regalbuto, J. R. (2005). *Phys. Rev. Lett.* **94**, 076104.
Parratt, L. G. (1954). *Phys. Rev.* **95**, 359–369.
Paulus, M., Gutt, C. & Tolan, M. (2005). *Phys. Rev. E*, **72**, 061601.
Paulus, M., Gutt, C. & Tolan, M. (2008). *Surf. Interface Anal.* **40**, 1226–1230.
Ravindra, R., Zhao, S., Gies, H. & Winter, R. (2004). *J. Am. Chem. Soc.* **126**, 12224–12225.
Reich, C., Hochrein, M. B., Krause, B. & Nickel, B. (2005). *Rev. Sci. Instrum.* **76**, 095103.
Reichert, H., Klein, O., Dosch, H., Denk, M., Honkimäki, V., Lippmann, T. & Reiter, G. (2000). *Nature (London)*, **408**, 839–841.
Rieutord, F., Eymery, J., Fournel, F., Buttard, D., Oeser, R., Plantevin, O., Moriceau, H. & Aspar, B. (2001). *Phys. Rev. B*, **63**, 125408.
Shokuie, K., Paulus, M., Sternemann, C., Fendt, R. & Tolan, M. (2007). *Thin Solid Films*, **515**, 5660–5663.
Sloutskin, E., Baumert, J., Ocko, B. M., Kuzmenko, I., Checco, A., Tamam, L., Ofer, E., Gog, T., Gang, O. & Deutsch, M. (2007). *J. Chem. Phys.* **126**, 054704.
Sosnick, T. R. & Trewhella, J. (1992). *Biochemistry*, **31**, 8329–8335.
Sternemann, C., Volmer, M., Soininen, J. A., Nagasawa, H., Paulus, M., Enkisch, H., Schmidt, G., Tolan, M. & Schülke, W. (2003). *Phys. Rev. B*, **68**, 035111.
Su, T. J., Lu, J. R., Thomas, R. K., Cui, Z. F. & Penfold, J. (1998). *Langmuir*, **14**, 438–445.
Svergun, D. I., Richard, S., Koch, M. H. J., Sayers, Z., Kuprin, S. & Zaccai, G. (1998). *Proc. Natl. Acad. Sci. USA*, **95**, 2267–2272.
Tikhonov, A. M., Patel, H., Garde, S. & Schlossman, M. (2006). *J. Phys. Chem. B*, **110**, 19093–19096.
Tolan, M. (1999). *Springer Tracts in Modern Physics*, Vol. 148, *X-ray Scattering from Soft Matter Thin Films.* Berlin: Springer.
Tolan, M., Weis, T., Westphal, C. & Wille, K. (2003). *Synchrotron Rad. News*, **16**, 9–11.
Winter, R. & Köhling, R. (2004). *J. Phys. Condens. Matter*, **16**, S327–S352.
Woenckhaus, J., Köhling, R., Thiyagarajan, P., Royer, C. A. & Winter, R. (2001). *Biophys. J.* **80**, 1518–1523.
Zhou, H.-X. & Dill, K. A. (2001). *Biochemistry*, **40**, 11289–11293.